Variational Blind Deconvolution of Multi-Channel Images

Ran Kaftory,[1] Nir Sochen,[2] Yehushua Y. Zeevi[1]

[1] Department of Electrical Engineering, Technion, Haifa 43000, Israel

[2] Department of Mathematics, Tel-Aviv University, Tel-Aviv 69978, Israel

Received 1 June 2004; accepted 2 April 2005

ABSTRACT: The fundamental problem of denoising and deblurring images is addressed in this study. The great difficulty in this task is due to the ill-posedness of the problem. We analyze multi-channel images to gain robustness and regularize the process by the Polyakov action, which provides an anisotropic smoothing term that uses inter-channel information. Blind deconvolution is then solved by an additional anisotropic regularization term of the same type for the kernel. It is shown that the Beltrami regularizer leads to better results than the total variation (TV) regularizer. An analytic comparison to the TV method is carried out and results on synthetic and real data are demonstrated. Int J Imaging Syst Technol, 15, 56–63, 2005; Published online in Wiley InterScience (www.interscience.wiley.com). DOI 10.1002/ima.20038

Key words: image restoration; color images; kernel estimation; variational methods; Non-linear PDEs

I. INTRODUCTION AND PREVIOUS WORK

Noisy images are a practical reality that pose a challenge to any front-end imaging and vision system. Noise is introduced due to thermal fluctuations in sensors, quantization effects, and properties of communication channels. Blurring occurs due to scattering of the light (e.g. atmosphere turbulence), optical limitations, and motion. The widely used model of spatially invariant linear blurring operator and additive Gaussian noise is adopted in this study to account for the blurring phenomena and the noise characteristics.

Denoting by $u^a(x, y)$, $a = 1, \ldots, d$, the source color channels of an image, the observed degraded color channel $z^a(x, y)$ is modeled as

$$z^a = h * u^a + n, \tag{1}$$

where $h(x,y)$ is a blurring kernel acting on u^a by convolution, n is a Gaussian white noise with zero mean and σ variance. The channels $a = r, g, b$ are taken here as the RGB basis for color space. Solving $\|h * u - z\|^2 = \sigma^2$ for u and h is an ill-posed problem, because of the nonuniqueness of the solution (Tikhonov and Arsenin, 1977).

Correspondence to: Prof. Nir Sochen; e-mail: sochen@post.tau.ac.il

Grant sponsors: Research supported in part by the Ollendorff Center, the Adams Brain Super-Center, The Israeli Academy of Science and the ONR-MURI Research Program.

One method of regularization, used for reconstructing gray value images, is the total variation (TV) blind deconvolution (Chan and Wong, 1998). This method suggests simultaneous recovery of the sharp denoised image and its blurring kernel. The recovery process is based on minimization of the functional

$$\min_{u,h} f(u,h) \equiv \min_{u,h} \left\{ \frac{1}{2} \|h * u - z\|^2 + \alpha_1 \mathrm{TV}(u) + \alpha_2 \mathrm{TV}(h) \right\}, \tag{2}$$

where we use the L^2 norm in the data term. The TV regularization operator is defined as

$$\mathrm{TV}(u) = \int |\nabla u| \, dx \, dy, \tag{3}$$

and it was successfully used for edge-preserving image denoising (Rudin et al., 1992).

A more general regularization operator was recently introduced in the context of the Beltrami framework for low-level vision (Sochen et al., 1997; Sochen et al., 1998). According to this framework, color images are represented as surfaces in R^5, with the coordinates (x, y, u^r, u^g, u^b). A metric is introduced for measuring distances on the surfaces, and minimization of the Polyakov action, adopted from high-energy physics, yields the Beltrami operator. In an Euclidean space, the Polyakov action (along with the induced metric) measures the surface area. Minimizing it causes the image to become smoother, its color channels to co-orient and align, and consequently, its edges to be preserved and match in position (Kimmel et al., 2000) and see Section VI later. This is much unlike the results of reconstruction by considering the three color channels independently. Another way of understanding it is via the regularization flow. The flow can be understood as an adaptive average. The support of a given gray value or color in a pixel comes from near-by pixels. The Beltrami flow gives higher influence to pixels that are near in lattice and *in color space*. In this way, pixels that

are near an edge are not influenced by the pixels in the other side of the edge even if they are close in the lattice. This way of measuring distances respects, thus, the edge and region structure of the image (Spira et al., 2005).

In this paper, the approach of minimizing a functional, resembling that of Eq. (2), is combined with the Polyakov action as a regularization operator, so as to deblur and denoise a blurred color image contaminated by Gaussian noise. The functional to be minimized is

$$\min_{u^a,h} f \equiv \min_{u^a,h}\left\{\frac{1}{2}\sum_a \|h * u^a - z^a\|^2 + \alpha_1 S(u^a) + \alpha_2 S(h)\right\}, \quad (4)$$

where the norms are in the L^2 sense, and S is the Polyakov action. Minimizing Eq. (4) with respect to u^r, u^g, u^b, and h, recovers the image-color channels and the blurring kernel, simultaneously. The parameters α_1 and α_2 control the degree of smoothness of the solution.

Alternatively, we will alternate the minimization of the image and the blurring kernel such that the following free energies are minimized:

$$\min_u f_u(\mathbf{u}; h, \mathbf{z}) \equiv \min_{u^a}\left\{\frac{1}{2}\sum_a \|h * u^a - z^a\|^2 + \alpha_1 S(\mathbf{u})\right\}, \quad (5)$$

$$\min_h f_h(h; \mathbf{u}, \mathbf{z}) \equiv \min_h\left\{\frac{1}{2}\sum_a \|h * u^a - z^a\|^2 + \alpha_2 S(h)\right\}. \quad (6)$$

The paper is organized as follows: we first introduce the main ideas regarding the Beltrami framework i.e., the representation of color images as 2D surfaces embedded in a 5D space, the induced metric for measuring distances on the surface and the Polyakov action, which measures the surface area. The numerical scheme for minimizing Eq. (4) (or equivalently Eqs. (5) and (6)), which is similar to the alternating minimization scheme, described by Chan and Wong (1998), is then presented. The Beltrami operator is incorporated into the Euler–Lagrange equations, by modifying the regularization parameters (or by adding a functional (Kaftory et al., Technical Report, in preparation)). The equations are linearized by the fixed-point lagged diffusive method, discussed by Vogel and Oman (1996), and solved using the conjugate-gradient method. The regularization parameters are then selected to provide the best possible results.

Finally, the properties of the Beltrami-based restoration are analyzed and illustrated by examples, and its advantages over other techniques are discussed.

II. IMAGES AS SURFACES EMBEDDED IN A HIGHER DIMENSIONAL SPACE

A color image is represented according to the Beltrami framework (Kimmel et al., 2000) as a 2D surface embedded in a 5D "spatial-feature" space via the "Monge patch" $(X^1, X^2, X^3, X^4, X^5) = (x, y, u^r, u^g, u^b)$. The blurring kernel can be similarly represented as a 2D surface embedded in a 3D "spatial-feature" space (x, y, h). The distance, ds, on the image surface, measured as a function of the local coordinates on the surface, is defined as follows:

$$ds^2 = g_{11}\,dx^2 + 2g_{12}\,dx\,dy + g_{22}\,dy^2, \quad (7)$$

where $G = (g_{\mu\nu})$ is a Riemannian metric. Let $X : \Sigma \to M$ be an embedding of Σ in M, where M is a Riemannian manifold with a metric $(k_{ab})_M$. We can use the knowledge of the metric on M and the map X to construct the metric on Σ. This procedure is called the pullback procedure and is given as follows:

$$(g_{\mu\nu})_\Sigma(\sigma^1, \sigma^2) = (k_{ab})_M(X(\sigma^1, \sigma^2))\ \partial_\mu X^a\ \partial_\nu X^b, \quad (8)$$

where $a, b = 1,\ldots,$ dim M are being summed over, and $\partial_\mu X^a \equiv \frac{\partial X^a(\sigma^1,\sigma^2)}{\partial\sigma^\mu}$.

For the 2D surface it is given explicitly as

$$\begin{aligned} g_{11} &= \sum_{a=1}^{n}\sum_{b=1}^{n} k_{ab}\frac{\partial X^a}{\partial x}\frac{\partial X^b}{\partial x}, \\ g_{12} = g_{21} &= \sum_{a=1}^{n}\sum_{b=1}^{n} k_{ab}\frac{\partial X^a}{\partial x}\frac{\partial X^b}{\partial y}, \\ g_{22} &= \sum_{a=1}^{n}\sum_{b=1}^{n} k_{ab}\frac{\partial X^a}{\partial y}\frac{\partial X^b}{\partial y}, \end{aligned} \quad (9)$$

where n is the dimension of the embedding space, and k_{ab} is its metric. Defining k_{ab} for the embedding color space, and for the embedding blurring kernel space, as (see other interesting options in Sochen and Zeevi, 1998)

$$k_{ab} = \begin{cases} \delta_{ab} & a, b = 1,2, \\ \beta^2\delta_{ab} & \text{elsewhere}, \end{cases} \quad (10)$$

and using the pullback procedure, the metric $G = g_{\mu\nu}$ can be calculated for the color surface and the blurring kernel surface respectively:

$$\begin{aligned} G_{rgb} &= \begin{pmatrix} 1 + \beta^2\sum_a (u_x^a)^2 & \beta^2\sum_a u_x^a u_y^a \\ \beta^2\sum_a u_x^a u_y^a & 1 + \beta^2\sum_a (u_y^a)^2 \end{pmatrix}, \\ G_h &= \begin{pmatrix} 1 + \beta^2 h_x^2 & \beta^2 h_x h_y \\ \beta^2 h_x h_y & 1 + \beta^2 h_y^2 \end{pmatrix}. \end{aligned} \quad (11)$$

The Polyakov action is defined for a generally defined metric embedding X^a and metric G as

$$S(X^a) = \int dx\,dy\,\sqrt{\det G}\sum_{ab}\nabla X^a G^{-1}\nabla X^b k_{ab}. \quad (12)$$

The modified gradient descent equations for this functional are (Sochen et al., 1998)

$$X_t^a = \Delta_G X^a = \frac{1}{\sqrt{\det(G)}}\nabla\left(\sqrt{\det(G)}G^{-1}\nabla X^a\right), \quad (13)$$

where $X_t^a \equiv \frac{\partial X^a}{\partial t}$.

For gray-valued and color images and their induced metrics, as described above, the functional Eq. (12) is reduced to an area functional

$$S(u^a) = \int \sqrt{\det G_{rgb}}\, dx\, dy = \int \sqrt{1 + \beta^2 \sum_a |\nabla u^a|^2 + \frac{1}{2}\beta^4 \sum_{ab} (\nabla u^a, \nabla u^b)^2}\; dx\, dy, \tag{14}$$

$$S(h) = \int \sqrt{\det G_{\ker}}\, dx\, dy = \int \sqrt{1 + \beta^2 |\nabla h|^2}\, dx\, dy, \tag{15}$$

where $(\bigtriangledown u^a, \bigtriangledown u^b)$ stand for the magnitude of the vector product of $\bigtriangledown u^a$ and $\bigtriangledown u^b$.

III. BELTRAMI-BASED RESTORATION

The Polyakov action is used as a regularization operator for both the color image and its blurring kernel. The functional to be minimized is as follows:

$$\min_{u^a,h} f \equiv \min_{u^a,h} \left\{ \frac{1}{2} \sum_a \|h * u^a - z^a\|^2 + \alpha_1 \int \sqrt{\det(G_{rgb})}\, dx\, dy + \alpha_2 \int \sqrt{\det(G_{\ker})}\, dx\, dy \right\}. \tag{16}$$

The Euler–Lagrange equations for Eq. (16), with respect to u^a and h, are given as follows:

$$\frac{\delta f}{\delta h} = \sum_a (u^a - x, -y * h * u^a - z^a) - \alpha_2 \nabla \cdot \left(\sqrt{\det(G_{\ker})} G_{\ker}^{-1} \nabla h \right) = 0,$$
$$\frac{\delta f}{\delta u^a} = h(-x, -y) * (h * u^a - z^a) - \alpha_1 \nabla \cdot \left(\sqrt{\det(G_{rgb})} G_{rgb}^{-1} \nabla u^a \right) = 0, \tag{17}$$

with the boundary conditions $\frac{\partial u^a}{\partial n} = 0$ and $h(x, y) = 0$ for $(x, y) \in \partial\Omega$, where $\partial\Omega$ is the boundary of the kernel domain, and n is the normal to the boundary of the image domain.

Since the extent of regularization is controlled by the regularization parameter, we want to diminish it near the edges. Since the term $\sqrt{\det(G)}$ is basically an edge indicator, we can use a similar idea to the adaptive TV minimization presented by Strong et al. (1997) and replace the regularization parameters α_1 and α_2 with the terms.

$$\alpha_1(x, y) \to \frac{\alpha_1}{\sqrt{\det(G_{rgb})}}, \quad \alpha_2(x, y) \to \frac{\alpha_2}{\sqrt{\det(G_h)}}. \tag{18}$$

The new definitions of the regularization parameters α_1 and α_2 introduce the natural generalization of the Laplacian from flat spaces to manifolds, and the so-called second order differential parameter of Beltrami to be denoted by Δ_G:

$$\frac{\delta f}{\delta h} = \sum_a u^a(-x, -y) * (h * u^a - z^a) - \alpha_2 \Delta_{G_{\ker}}(h) = 0,$$
$$\frac{\delta f}{\delta u^a} = h(-x, -y) * (h * u^a - z^i) - \alpha_1 \Delta_{G_{rgb}}(u^a) = 0, \tag{19}$$

with the boundary conditions as in (17), where $\Delta_G(X) = \frac{1}{\sqrt{\det(G)}} \nabla \cdot \sqrt{\det(G)} G^{-1} \nabla X$.

The functional $f(u^r, u^g, u^b, h)$ in Eq. (16) is not jointly convex. But, for a given u^r, u^g, and u^b it is convex with respect to h. For a given u^g, u^b, and h, $f(\cdot, u^b, u^g, h)$ is a convex function with respect to u^r and similarly for u^g and u^b. This enables the adaptation of the alternating minimization scheme, which was found to be robust and fast (Chan and Wong, 1999).

The Eq. (19) can be derived alternatively by minimizing two functionals. Similarly, the image and the kernel are described as surfaces embedded in a higher dimensional Euclidean space. The metric of the Euclidean space is k_{ab} as described earlier. The fidelity term is defined then on the manifold:

$$\min_{u^a,h} f_u \equiv \min_{u^a} \left\{ \frac{1}{2} \sum_a \int dx\, dy \sqrt{G_{rgb}} \|h * u^a - z^a\|^2 + \alpha_1 \int dx\, dy \sqrt{\det(G_{rgb})} G_{rgb}^{ij} \nabla_i X^a \nabla_j X^a \right\}, \tag{20}$$

$$\min_{u^a,h} f_h \equiv \min_{h} \left\{ \frac{1}{2} \sum_a \int dx\, dy \sqrt{G_{\ker}} \|h * u^a - z^a\|^2 + \alpha_2 \int dx\, dy \sqrt{\det(G_{\ker})} G_{\ker}^{ij} \nabla_i X^a \nabla_j X^a \right\}. \tag{21}$$

The modified Euler–Lagrange equations are

$$\frac{1}{\sqrt{G_{rgb}}} \frac{\delta f_u}{\delta u^a} = 0, \quad \frac{1}{\sqrt{G_{\ker}}} \frac{\delta f_h}{\delta h} = 0 \tag{22}$$

and are identical to Eq. (19). Note that the fidelity term is weighted in these functionals by a locally dependent factor. This means that at each point the relation between the smoothing part and the fidelity part is different. In particular, the fidelity to the measurements is enforced strongly at points with high gradients where the determinant of the metric is large. Larger deviations from the observations are permissible at points with low gradients. In the modified Euler–Lagrange equations, the factor $\sqrt{\det(G)}$ is shifted to the smoothing term. This amounts for an adaptive smoothing mechanism: At points of large gradients, the smoothing term is suppressed and fidelity of the restored image to the observed values is enforced. Larger smoothing is allowed to take place at points of low-gradient values.

The minimization scheme is stated as follows: Take as initial guess, $u^{a_0} = z^a$ and $h^0 = \delta(x, y)$. Assume we have u^{a_n} and h^n, and solve for h^{n+1},

$$\sum_a u^{a_n}(-x, -y) * (h^{n+1} * u^{a_n} - z^a) - \alpha_2\, \Delta_{G_{\ker}}(h^{n+1}) = 0, \tag{23}$$

and impose the following conditions over the solution: $\int_\Omega h^{n+1}(x,y)\,dx\,dy = 1$, $h^{n+1}(x,y) = h^{n+1}(-x,-y), h^{n+1}(x,y) \geq 0$, and $h^{n+1}(x,y) = 0$ for $(x,y) \in \partial\Omega$.

Solve for $u^{a_{n+1}}$:

$$h^{n+1}(-x,-y) * (h^{n+1} * u^{a_{n+1}} - z^a) - \alpha_1 \Delta_{G_{rgb}}(u^{a_{n+1}}) = 0 \qquad (24)$$

and impose the following condition $u^{a_{n+1}}(x, y) \geq 0$ over the solution.

The proposed algorithm can be modified to solve first for $u^{a_{n+1}}$ and then for h^{n+1}. The Euler–Lagrange equations are linearized using the fixed-point lagged diffusive method, introduced in (Vogel and M. Oman, 1996) and solved using the conjugate gradient methods described in (Hanke, 1995).

IV. REGULARIZATION PARAMETERS

The parameter β, introduced in the induced metric in section II, interpolates between the Euclidean L_1 and Euclidean L_2 norms for the gradient's magnitude. Since the Euclidean L_2 norm penalizes discontinuities, and therefore prefers smooth restoration, we explore the more interesting case of a large β (Euclidean L_1 norm).

The regularization parameters α_1 and α_2 control the balance between goodness of fit of $h * u^a$ to the measured data z^a and the amount of regularization with respect to the Polyakov action of u^a and h. Intuitive, analytic, and numerical considerations can lead to the choice of values for the regularization parameters for the restored color image and the blurring kernel.

A. The Parameter α_1 As was described earlier, the Polyakov action measures the surface area of the manifold. Color image is a 2D surface embedded in a 5D space. Minimizing its surface area will de-noise the image, since noise is a feature with very large surface area in comparison to its scale.

The first step of the restoration scheme can be solving Eq. (24) first and then Eq. (23). Inserting the initial guess $h^0 = \delta(x, y)$, Eq. (24) yields

$$(u^{a_1} - z^a) - \alpha_1 \Delta_{G_{rgb}}(u^{a_1}) = 0. \qquad (25)$$

The problem in this step is reduced by finding the best regularization parameter for denoising a color channel u^{a1} when blur is not introduced.

This parameter was found to be proportional to the noise variance and by numerical experiments, it was found that setting it to the noise variance is adequate (Kaftory, 2001).

B. The Parameter α_2 Unlike the case of the regularization parameter α_1, in which the problem was reduced by finding the best regularization parameter for denoising a color image when blur is not introduced, the case for finding the regularization parameter α_2 is not that simple. The analytic tools used so far for finding the regularization parameter for the color image are not adequate for finding the best regularization parameter for the kernel. Intuition and previous work (Chan and Wong, 1998) suggest that the parameter does not depend on the noise level of the image, but depends on the extent of the desired deblurring.

Experiments show that there is a wide range of values for α_2 (from 0.01 to 0.05) that estimate the same kernel. Within this range, the estimated kernel depends only on the extent of blurring, affecting the observed image (Kaftory, 2001).

V. RESULTS

The proposed algorithm was found to be robust. It converges after only five iterations. Figures 1–4 illustrate examples of restoration of color images blurred by Gaussian, motion and out-of-focus kernels and degraded by Gaussian noise. The restoration uses the regularization parameters determined in the previous section. Observe how the restored images are sharp and noiseless, and the estimated blurring kernels resemble the true kernels.

A quantitative measure of the error, associated with the estimation of the color image and of the blurring kernel, can be obtained by calculating the peak signal-to-noise ratio (PSNR).

$$\mathrm{PSNR}(X) = 20 \log \sqrt{\frac{3N \cdot M}{\sum_a \sum_{j=1}^{N} \sum_{k=1}^{M} (X^a_{j,k} - \hat{X}^a_{j,k})^2}},$$

where X stands for u^a or h, and $N \cdot M$ is the number of pixels. Table I summarizes the PSNR of the images in Figures 1–4.

VI. PROPERTIES OF THE BELTRAMI-BASED RESTORATION

The properties of restoration of a 2D surface, embedded in a 3D "spatial-feature" space, similar to the case of gray-value images (or the blurring kernel) are explored first. The Polyakov action in Eq. (14) becomes (for a large β) the modified TV operator defined by Vogel and Oman (1996) as

$$S(h) = \int \sqrt{1 + \beta^2 (\nabla h)^2}\,dx\,dy = \beta \int \sqrt{\gamma^2 + (\nabla h)^2}\,dx\,dy = \beta\ \mathrm{TV}(h), \qquad (26)$$

where $\gamma = \frac{1}{\beta}$.

Since the TV does not penalize discontinuities or smooth monotone functions, it was used successfully as a regularization operator in reconstructing gray-valued images (Rudin et al., 1992; Chan and Wong, 1998). Reconstruction using the TV operator was explored by Strong and Chan (2000) and yielded the following properties: edges are preserved in the reconstructed image; the intensity change of image features is proportional to the regularization parameter, and inversely proportional to the feature scale; small-scale details, like noise, are smoothed out, leaving a sharp noiseless reconstruction. In the Beltrami-based restoration, the regularization parameter α_1 is replaced in the Euler–Lagrange equation by $\frac{\alpha_1}{\sqrt{\det(G)}}$, yielding an adaptive TV restoration (Strong, 1997). Since the term $\frac{\alpha_1}{\sqrt{\det(G)}}$ is basically an edge indicator, it assumes small values in the presence of an edge, while in smooth areas, in which the gradients are very close to zero, its values increase up to one. This feature overcomes the problems of the intensity reduction near edges, and of elimination of small-scale features. To illustrate this property, consider the simple R^1 function

$$u(x) = \begin{cases} 0.2 & x \in \Omega_1, \\ 0.8 & x \in \Omega_2, \\ 0.2 & x \in \Omega_3. \end{cases} \qquad (27)$$

A Gaussian noise is added to this function to produce the noisy function

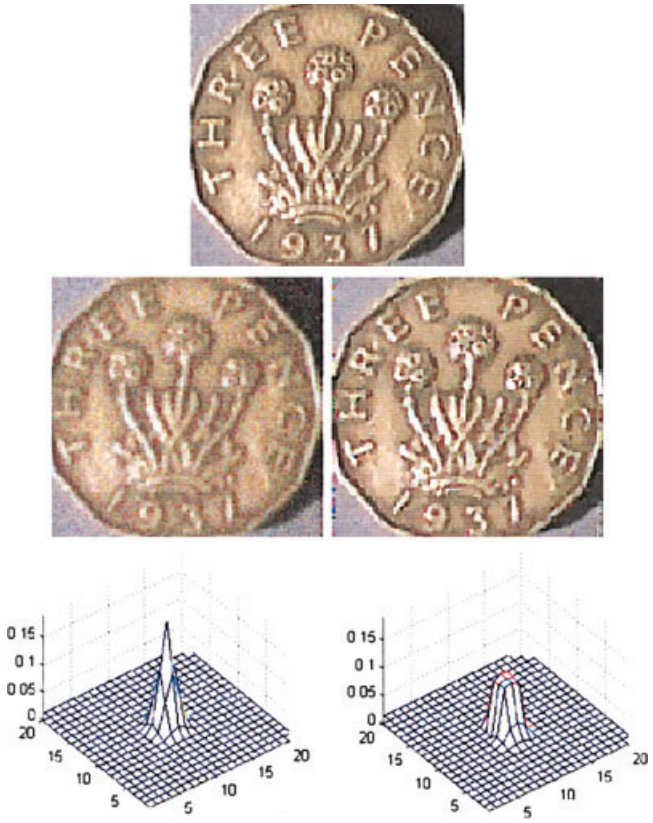

Figure 1. Radially symmetric blur. From left to right: 1st row, original; 2nd row, blurred and noisy image, restored image; 3rd row, true and estimated kernels.

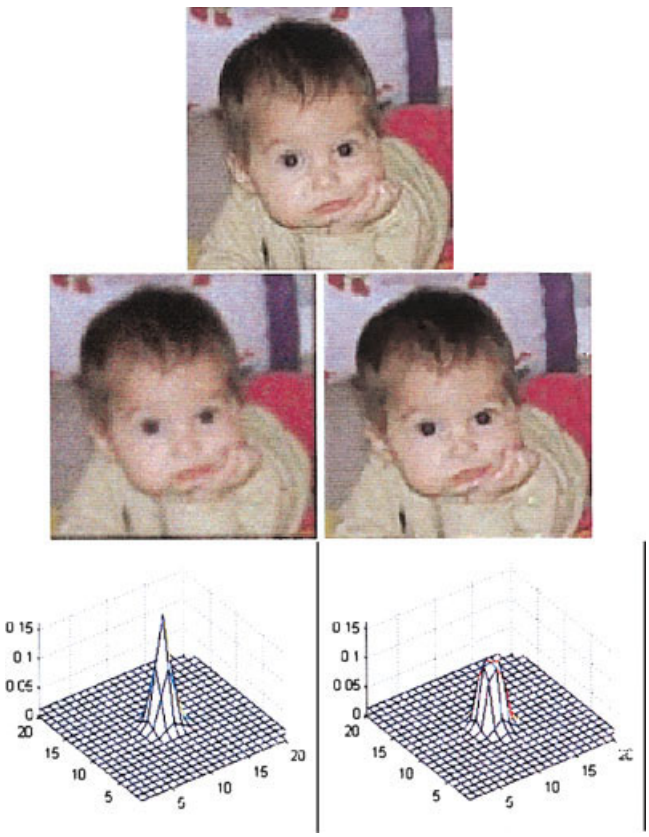

Figure 2. Radially symmetric blur. From left to right: 1st row, original; 2nd row, blurred and noisy image, restored image; 3rd row, true and estimated kernels.

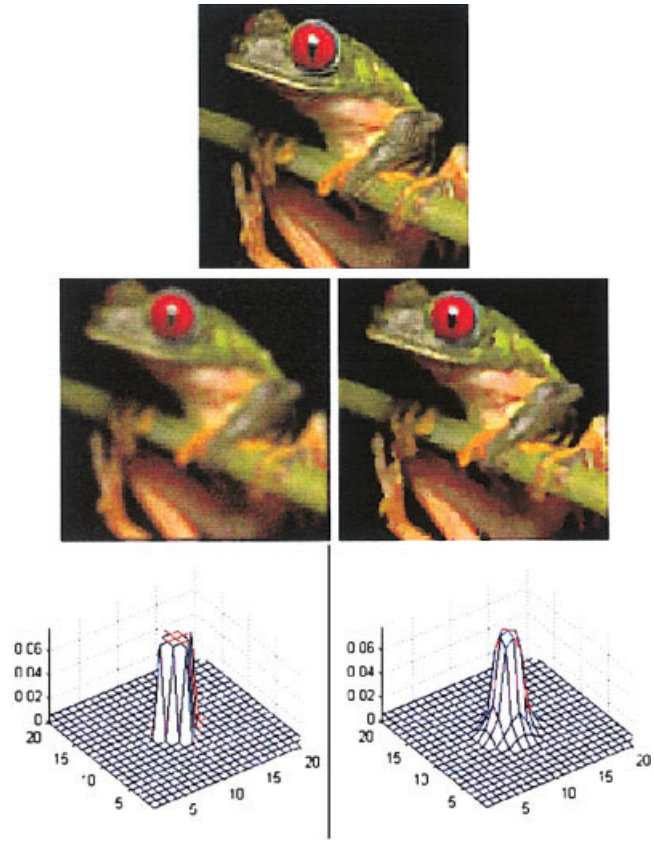

Figure 3. Out of focus blur. From left to right: 1st row, original; 2nd row, blurred and noisy image, restored image; 3rd row, true and estimated kernels.

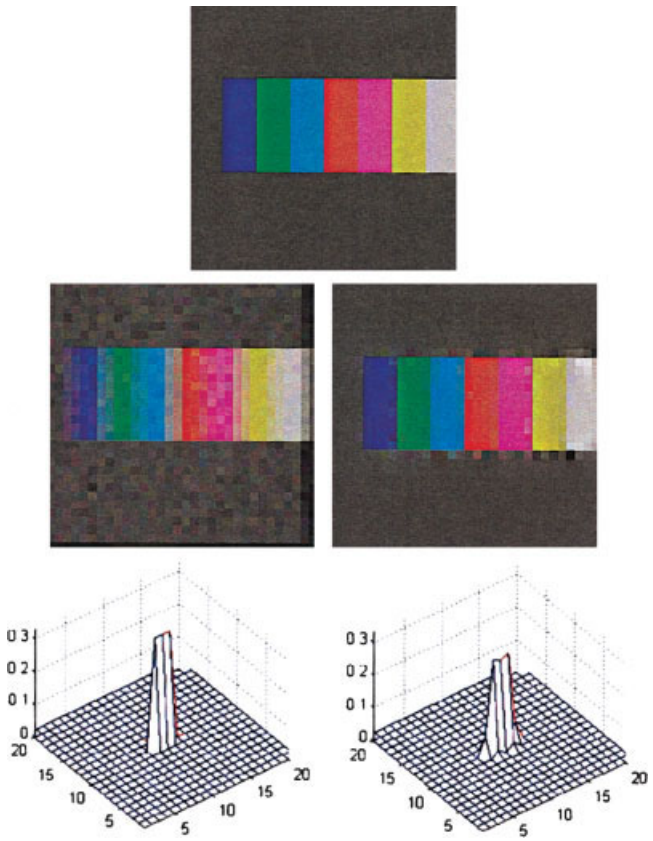

Figure 4. Motion blur. From left to right: 1st row, original; 2nd row, blurred and noisy image, restored image; 3rd row, true and estimated kernels.

Table 1. PSNR (in dB) of the restored images and kernels.

Image	Observed Image PSNR	Restored Image PSNR	Restored Kernel PSNR
Coin	21	23	60
Baby	28	32	62
Frog	25	27	59
Color bar	24	31	47

$$z(x) = u(x) + n. \tag{28}$$

Experiment with the Beltrami-based restoration algorithm on this noisy function suggests that the restored function should be

$$u(x) = \begin{cases} 0.2 + \delta_1 & x \in \Omega_1, \\ 0.8 + \delta_2 & x \in \Omega_2, \\ 0.2 + \delta_3 & x \in \Omega_3, \end{cases} \tag{29}$$

where δ_i is the intensity change in region i. The restoration problem is given as follows:

$$\min_u \left\{ \frac{1}{2}\|u-z\|^2 + \alpha_1 \beta \, \mathrm{TV}(u) \right\} = \min_{\delta^i} \left\{ \sum_i \left(|\Omega_i| \delta_i^2 \right) + \alpha_1 \beta (0.6 + \delta_2 - \delta_1 + 0.6 + \delta_2 - \delta_3) \right\}, \tag{30}$$

where $|\Omega_i|$ is the length of region i. Minimizing Eq. (30) by derivation with respect to δ^i yields

$$\delta_1 = \frac{\alpha_1 \beta}{|\Omega_1|}, \quad \delta_2 = \frac{2\alpha_1 \beta}{|\Omega_2|}, \quad \delta_3 = \frac{\alpha_1 \beta}{|\Omega_3|}. \tag{31}$$

Therefore, in the restored function $u(x)$, the intensity change is directly proportional to the parameter α_1 and inversely proportional to the scale. This result was presented in (Strong, 1997) for the TV-based restoration.

For simplicity, let us assume that $|\Omega_1| = |\Omega_3|$, and therefore $\delta_1 = \delta_3$. Modifying the regularization parameter α_1 to $\frac{\alpha_1}{\sqrt{\det(G)}} = \frac{\alpha_1}{\sqrt{1+\beta^2|\nabla u|^2}}$, introduces the Beltrami operator to the solution. The regularization parameter can be explicitly expressed by

$$\frac{\alpha_1}{\sqrt{1+\beta^2|\nabla u|^2}} = \begin{cases} \frac{\alpha_1}{\sqrt{1+\beta^2(0.6+\delta_2-\delta_1)^2}} & x \in \partial_{12}, \\ \frac{\alpha_1}{\sqrt{1+\beta^2(0.6+\delta_2-\delta_1)^2}} & x \in \partial_{23}, \\ \alpha_1 & \text{elsewhere}, \end{cases} \tag{32}$$

where ∂_{12} stands for the boundary of region 1 and 2, and ∂_{23} stands for the boundary of region 2 and 3.

Considering only the boundary points and implementing the modified α_1, Eq. (31) becomes

$$\begin{aligned} \delta_1 &= \frac{\alpha_1 \beta}{|\Omega_1|\sqrt{1+\beta^2(0.6+\delta_2-\delta_1)^2}} \quad (\text{on } \partial_{12}), \\ \delta_2 &= -\frac{2\alpha_1 \beta}{|\Omega_2|\sqrt{1+\beta^2(0.6+\delta_2-\delta_1)^2}} \quad (\text{on } \partial_{12}), \\ \delta_2 &= -\frac{2\alpha_1 \beta}{|\Omega_2|\sqrt{1+\beta^2(0.6+\delta_2-\delta_1)^2}} \quad (\text{on } \partial_{23}), \\ \delta_3 &= \frac{\alpha_1 \beta}{|\Omega_1|\sqrt{1+\beta^2(0.6+\delta_2-\delta_1)^2}} \quad (\text{on } \partial_{23}). \end{aligned} \tag{33}$$

Since β is assumed to be very large, Eq. (33) can be approximated as follows:

$$\begin{aligned} \delta_1 &= \frac{\alpha_1}{|\Omega_1|(0.6+\delta_2-\delta_1)} \quad (\text{on } \partial_{12}), \\ \delta_2 &= -\frac{2\alpha_1}{|\Omega_2|(0.6+\delta_2-\delta_1)} \quad (\text{on } \partial_{12}), \\ \delta_2 &= -\frac{2\alpha_1}{|\Omega_2|(0.6+\delta_2-\delta_1)} \quad (\text{on } \partial_{23}), \\ \delta_3 &= \frac{\alpha_1}{|\Omega_1|(0.6+\delta_2-\delta_1)} \quad (\text{on } \partial_{23}). \end{aligned} \tag{34}$$

Since $\delta_1 = \delta_3$ the solution to (34) is

$$\begin{aligned} \delta_1 &= \frac{0.6|\Omega_1||\Omega_2| - \sqrt{|\Omega_1|^2|\Omega_2|^2 0.36 - 4|\Omega_2|(|\Omega_1||\Omega_2| + 2|\Omega_1|^2)\alpha_1}}{2(|\Omega_1||\Omega_2| + 2|\Omega_1|^2)}, \\ \delta_2 &= -\frac{0.6|\Omega_1||\Omega_2| - \sqrt{|\Omega_1|^2|\Omega_2|^2 0.36 - 4|\Omega_2|(|\Omega_1||\Omega_2| + 2|\Omega_1|^2)\alpha_1}}{(|\Omega_2|^2 + 2|\Omega_1||\Omega_2|)}. \end{aligned} \tag{35}$$

In this case, intensity change δ_i is not directly proportional to the regularization parameter α_1 or inversely proportional to the scale in the boundary points. In fact the intensity change is minimal.

The function z is actually divided into two types of regions. Step regions in which the intensity change is defined in (35), and smooth regions in which the parameter

$$\frac{\alpha_1}{\sqrt{1+\beta^2 \, |\nabla u|^2}} \approx \alpha_1,$$

and the intensity change are defined in Eq. (31).

Restoration of the function u using the TV operator and the Beltrami operator are shown in Figure 5. Gaussian noise with variance 0.05 was added to the function u. The size of the regions is $|\Omega_1| = |\Omega_3| = 25$, $|\Omega_2| = 10$, $\alpha_1 = 1/60$ and $\beta = 60$.

The TV restoration should yield

$$\delta_1 = \delta_3 = \frac{\alpha_1 \beta}{25} = 0.04, \quad \delta_2 = -\frac{\alpha_1 \beta}{5} = -0.2, \tag{36}$$

and the Beltrami-based restoration should yield

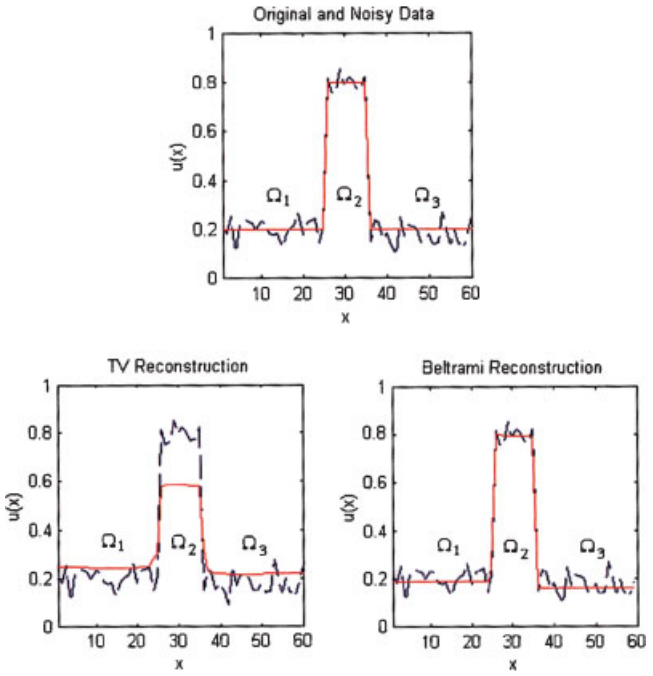

Figure 5. Original noisy image. Down-left: After denoising by TV. Down-right: After denoising with the Beltrami operator.

$$\delta_1 = \delta_3 = \frac{150 - \sqrt{22500 - 60000\alpha_1}}{3000} = 0.001,$$
$$\delta_2 = -\frac{150 - \sqrt{22500 - 60000\alpha_1}}{600} = -0.005. \qquad (37)$$

Observe the contrast reduction between Ω_1 and $\Omega_2/3$ in the TV-based restoration (caused by the direct relation to the smoothing parameter α_1). The value of Ω_2 is extensively reduced because of its small scale (caused by the inverse relation to the feature scale). In the Beltrami-based restoration, the change in the contrast is hardly seen because of the wick relation to α_1 and the feature scale. The numerical results, as seen in Figure 5, match perfectly with the analytic prediction of Eqs. (36) and (37).

As mentioned in Section II, the Polyakov action for a 2D surface embedded in a 5D "space-feature" space as in the case of a color image is

$$S(u^i) = \int \sqrt{G_{rgb}}\, dx\, dy$$
$$= \int \sqrt{1 + \beta^2 \sum_a \left(|\nabla u^a|^2\right) + \frac{1}{2}\beta^4 \sum_{ab} (\nabla u^a, \nabla u^b)^2}\, dx\, dy, \qquad (38)$$

where $(\bigtriangledown u^a, \bigtriangledown u^b)$ stands for the magnitude of the vector product of the vectors $\bigtriangledown u^a$ and $\bigtriangledown u^b$. While minimizing the Polyakov action, the term $1 + \beta^2 \sum_a |\nabla u^a|^2$ regularizes each color channel, as described in the gray-value case earlier. The term $\beta^4 \Sigma_{ab} (\bigtriangledown u^a, \bigtriangledown u^b)^2$, which is more dominant in the limit of a large β, measures the directional difference of the gradients between color channels. The minimization of the Polyakov action takes care, therefore, of the alignment and location matching of the edges over the three channels. To illustrate this, a noisy color image was produced by a digital camera (Fig. 6 up-left). The angles between the orientations

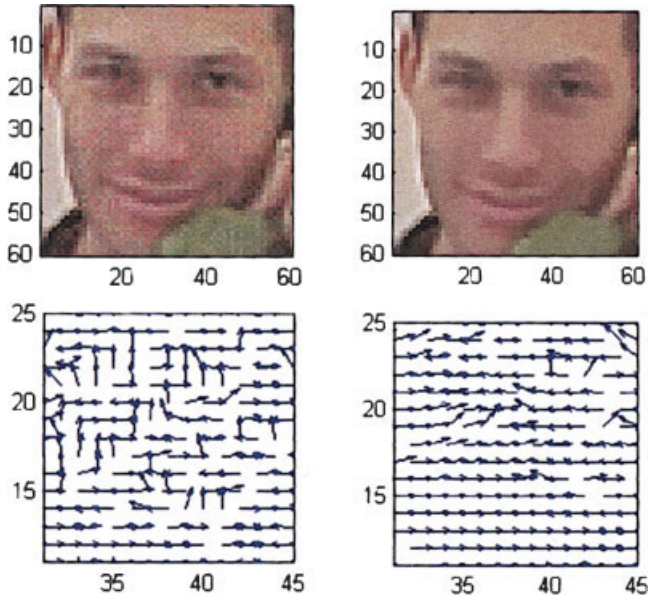

Figure 6. Up–down, left to right: original noisy image, denoised image, the angles between color gradients before, and after the denoising process.

of the gradient in the noisy image are plotted by arrows (Fig. 6 down-left). When an arrow points right the angle is zero (the gradients are of the same orientation). A Beltrami-based restoration is illustrated on the upright side of Figure 6. Note that in the original image the gradient of the channels do not align together, the image looks noisy, and the edges are not sharp. In the restored image, however, the angles between the gradient orientations are reduced (Fig. 6 down-right) and the restored image looks sharper and less noisy.

Color image reconstruction is hardly addressed, owing to the common belief that color image reconstruction can be treated as

Figure 7. Left to right, top to bottom: original, noisy, TV and Beltrami images.

Table 2. PSNR (in dB) of the TV and Beltrami restored image.

Observed Image PSNR	TV-Restored PSNR	Beltrami-Restored PSNR
23	29	30

reconstructing three gray-valued independent channels. This is a wrong assumption in applications in which the human visual system (HVS) is the receiver. The HVS is very sensitive to the slightest edge misalignment, or to intensity reduction in one of the color channels. Blomgren and Chan (1998) reported that the color TV was defined as a regularization operator for the restoration of vector-valued images. A coupling between the color channels was achieved through the regularization parameter, assigning small regularization parameter to channels with smaller TV. In the reconstructed color image, "weaker" channels are smoothed less, and therefore preserve the intensity relationship between the channels. In the Beltrami-based restoration, a coupling between the color channels is introduced not only through the regularization parameter but also through the regularization operator itself. Comparison between the best color TV reconstruction and the best Beltrami-based reconstruction of a noisy image, in which blur is not introduced, is depicted in Figure 7. Table II summarized the PSNR of these images. Observe how in both the reconstructed images, the noise is removed completely. However, only in the Beltrami-based reconstruction the edges are sharp and visually satisfying and color artifacts are not introduced. The blur and color artifacts in the TV process are caused probably because of misalignment of the edges in the different color channels (Tschumperlé, 2002).

VII. CONCLUDING REMARKS

Using the Beltrami operator in the objective functional, and adopting the alternating minimization scheme for minimizing Eq. (4), yields a robust algorithm for simultaneous recovery of a blurred noisy color image and of its blurring kernel. The parameters α_1 and α_2 of this process are automatically selected to yield good results. The restored images depict sharp edges and the gradients of the channels are well aligned. The RGB color space was adopted in this study. However, the approach can incorporate just as well the HVS color coordinates (Wolf et al., 1996). The HVS color space was shown to be effective in spatio-chromatic image enhancement. Another issue to be further explored relates to question of what is the "right" metric for measuring distances in the higher dimensional space (Sochen and Zeevi, 1998). Further such insight will most likely improve the results of the proposed approach to image deblurring and denoising.

REFERENCES

P. Blomgren and T. Chan, Color TV: Total variation method for restoration of vector-valued images, IEEE Trans Image Process 7 (1998), 304–309.

T. Chan and C. Wong, Convergence of the alternating minimization algorithm for blind deconvolution, CAM Report 99-19, UCLA Math Department, June, 1999.

T.F. Chan and C. Wong, Total variation blind de-convolution, IEEE Trans Image Process 7 (1998), 370–375.

M. Hanke, Conjugate gradient type methods for ill-posed problems, Longman Scientific & Technical, England, 1995, pp. 13.

R. Kaftory, Color image reconstruction using the Beltrami framework, M.Sc. Thesis, Technion—Israel Institute of Technology, Hiafa, 2001.

R. Kimmel, R. Malladi, and N. Sochen, Images as embedded maps and minimal surfaces: Movies, color, texture and volumetric medical images, Int J Comput Vis 39 (2000), 111–129.

L. Rudin, S. Osher, and E. Fatemi, Nonlinear total variation based noise removal algorithms, Physica D 60 (1992), 259–268.

N. Sochen, R. Kimmel, and R. Malladi, From high energy physics to low-level vision, In Lecture notes in computer science, Springer-Verlag, 1997. First Int Conf on Scale-Space Theory in Computer Vision, Utrecht, Netherlands, July 2–4, 1997.

N. Sochen, R. Kimmel, and R. Malladi, A general framework for low-level vision, IEEE Trans Image Process 7 (1998), 310–318.

N. Sochen and Y.Y. Zeevi, Representation of colored images by manifolds embedded in higher dimensional non Euclidean space, Proc of ICIP98, Chicago, 1998, pp. 166–170.

A. Spira, N. Sochen, and R. Kimmel, Geometric filters, diffusion flows, and kernels in image processing, In Eduardo Bayro-Corrochano (Editor), Handbook of computational geometry for pattern recognition, computer vision, neurocomputing and robotics, Springer-Verlag, Berlin, 2005, pp. 203–230.

D. Strong, Adaptive total variation minimizing image restoration, Ph.D. Dissertation, University of California, Los Angeles, (CAM Report 97-38), August, 1997.

D. Strong, P. Blomgren, and T. Chan, Spatially adaptive local feature-driven total variation minimizing image restoration, CAM Report 97-32, UCLA Math Department, July, 1997.

D. Strong and T. Chan, Edge-preserving and scale-dependent properties of total variation regularization, CAM Report 00-38, UCLA Math Department, October, 2000.

A. Tikhonov and V. Arsenin, Solutions of ill-posed problems, Winston & Sons, New York, 1977.

D. Tschumperlé, PDE-Based Regularization of Multivalued Images and Applications, Ph.D. Thesis, University of Nice, Sophia Antipolis, December, 2002.

C. Vogel and M. Oman, Iterative methods for total variation denoising, SIAM J Sci Comput 17 (1996), 227–238.

S.G. Wolf, R. Ginosar, and Y.Y. Zeevi, Spatio-chromatic image enhancement based on a model of human visual information processing, J. Visual Commun Image Rep 9 (1996), 25–37.